Generation of plasma zonal flow shear by finite parallel wave length density fluctuations in slab geometry

Y. Lang[1] and Z.B. Guo[1,*]

[1]School of Physics and State Key Lab of Nuclear Physics and Technology, Peking University, Beijing 100871, China

(Dated: December 27, 2020)

A possible zonal flow shear generation mechanism by drift wave turbulence in a cylindrical magnetized plasma with large relative density fluctuations is discussed. These fluctuations would introduce nonlinear terms in the vorticity equation other than the term related to Reynolds stress in Hasegawa-Wakatani equations. We show that a nonlinear term can explain the generation of zonal flow in a simulation of a linear magnetized plasma device. The simulated growth of zonal flow and profile of time-averaged Reynolds stress is compared to experimental observations. We thus show that in these experiments, when the relative density fluctuation is large, Reynolds force may not be the only mechanism for zonal flow generation.

I. INTRODUCTION

The generation of zonal flow (ZF) in magnetically confined plasma is of wide interest, since it can impact the instabilities and turbulence and thus transport, especially at the edge of tokamaks [1]. Through nonlinear interactions, energy can be transferred from drift waves (DW) to ZF [2]. Whereas the mechanism of turbulent momentum transport, especially through the Reynolds stress term in the stress tensor, is extensively studied, other mechanisms can also be important in certain conditions [3, 4].

For the study of ZF generation by collisional drift waves (CDW), the Controlled Shear Decorrelation Experiment (CSDX) with insulating endplates [5] is a promising testbed, in that it is a simple drift wave-zonal flow system [6, 7] in uniform magnetic field and shares many similar scaling properties with tokamak boundaries [8]. Experiments on CSDX find nonlinear kinetic energy transfer from weak CDW turbulence to ZF [6, 9] and ZF driven by Reynolds force [10–12]. These works explains ZF generations in CSDX, with systematic sources of error, such as the neglect of electron temperature fluctuations in converting floating potential measured by Langmuir probes to plasma potential, which is used to calculate electric field and fluid velocity [9, 10]. Consequently, it can be helpful to do similar analysis in simulations.

Recently two 3D codes based on drift-reduced two-fluid cold-ion equations have focused on the simulations of CSDX $B = 1000$ G insulating end-plates discharges [13, 14] and compared to experimental observations. The code under BOUndary Turbulence (BOUT++) framework [13] show considerable difference between actual (using plasma potential) and synthetic (using floating potential) Reynolds stress in the simulations, but do not quantitatively analyze the ZF generation in their simulations. In this paper, based on our flux-driven simulation [14], we do detailed analysis on ZF generation in our simulated system.

* E-mail:zbguo@pku.edu.cn

II. THEORETICAL MODEL

The system we are interested is a cylindrical plasma column in a uniform magnetic field $\boldsymbol{B} = B\hat{\boldsymbol{z}}$. The equilibrium of a given scalar field is its zonal average $\langle f\rangle \equiv \int_0^{L_\parallel}\int_0^{2\pi} f(r,\theta,z)\,d\theta dz$ and its fluctuation is $\delta f \equiv f - \langle f\rangle$, where $L_\parallel$ is the parallel wavelength of the DW. We use cold-ion and low-β limit, so ion temperature and magnetic perturbations are neglected.

A. vorticity equation

The drift-reduce two-fluid vorticity equation comes from the continuity equations and quasi-neutrality, with the form of charge conservation [15]

$$\nabla\cdot(n\boldsymbol{v}_p) + \nabla_\parallel j_\parallel = 0\ , \tag{1}$$

where

$$\boldsymbol{v}_p = -\frac{ec}{B\Omega_i} d_t \nabla_\perp\phi \tag{2}$$

is the ion polarization drift. $\Omega_i \equiv eB/(m_i c)$ is the constant ion gyro-frequency. $d_t \equiv \partial_t + \boldsymbol{v}_E\cdot\nabla$ is the total time derivative. In this paper we adopt Boussinesq approximation [16] to simplify the divergence of perpendicular current

$$\nabla\cdot(n d_t\nabla_\perp\phi) \approx n d_t \nabla_\perp^2\phi\ , \tag{3}$$

which allows us to define vorticity by

$$w\hat{\boldsymbol{z}} \equiv \nabla\times\boldsymbol{v}_E = \frac{c}{B}\nabla_\perp^2\phi\hat{\boldsymbol{z}}\ . \tag{4}$$

Discussions about gyro-fluid non-Boussinesq ZF generation can be found [17]. The zonal average of vorticity equation Eq. (1) is thus

$$\begin{aligned}\langle n\rangle\partial_t\langle w\rangle = &-\langle n\rangle\langle\delta\boldsymbol{v}_E\cdot\nabla\delta w\rangle\\ &-\left\langle\delta n\left(\partial_t + \langle v_{E,\theta}\rangle\frac{1}{r}\partial_\theta\right)\delta w\right\rangle\\ &+\langle\delta n\delta\boldsymbol{v}_E\cdot\nabla w\rangle\ .\end{aligned} \tag{5}$$

The first term on the right hand side (RHS) is the divergence of vorticity flux, which is the contribution of perpendicular Reynolds force to ZF, by the Taylor identity [18, 19]. This ZF generation mechanism has been extensively studied on CSDX [10–12, 20] and is the only mechanism in Hasegawa-Wakatani systems [7, 21]. The second term on the RHS can be neglected only when density fluctuations are small, i.e.

$$\frac{\delta n}{\langle n\rangle} \ll \frac{\omega_{nl}}{\omega}, \tag{6}$$

where $\omega_{nl} \equiv \delta\boldsymbol{v}_E \cdot \nabla$ is the nonlinear frequency and $\omega \equiv \partial_t + \langle v_{E,\theta}\rangle (1/r)\,\partial_\theta$ is the DW frequency Doppler shifted by ZF. If this condition is not satisfied, we have to retain density fluctuation in the ion polarization current in Eq. (1). Including ion-ion collisional viscosity $\mu_\perp$ and ion-neutral drag $\nu_{i,n}$ [22], the vorticity equation we use in our simulation [14] is

$$\partial_t w = -\boldsymbol{v}_E \cdot \nabla w + \frac{\Omega_i}{e}\frac{1}{n}\nabla_\parallel j_\parallel \ . \tag{7}$$

We use periodic parallel boundary condition and define the zonal-average of a given scalar field f by $\langle f\rangle \equiv \int_0^{L_\parallel}\int_0^{2\pi} f(r,\theta,z)\, d\theta dz$ and perturbation by $\delta f \equiv f - \langle f\rangle$. Taking zonal average of Equation (7), the LHS becomes

$$\begin{aligned}\left\langle \partial_t \nabla_\perp^2 \phi\right\rangle &= \partial_t\left[\frac{1}{r}\partial_r\left(r\langle v_{E,\theta}\rangle\right)\right] \equiv S^\dagger \\ &\approx \partial_t\left(\partial_r\langle v_{E,\theta}\rangle\right) \equiv S \ .\end{aligned} \tag{8}$$

In the second step we use the approximation $\partial_r \gg 1/r$, so this term becomes the evolution of zonal flow (ZF) shear. The first term on the RHS becomes

$$\begin{aligned}\left\langle -\boldsymbol{v}_E \cdot \nabla w\right\rangle &= -\partial_r\left\langle v_{E,r}\frac{1}{r}\partial_r\left(r v_{E,\theta}\right)\right\rangle \equiv F_\perp^\dagger \\ &\approx -\partial_{rr}^2\left\langle v_{E,r} v_{E,\theta}\right\rangle \equiv F_\perp \ ,\end{aligned} \tag{9}$$

where in the second step we use the approximation $\partial_r \gg 1/r$ for two times, and yield the radial derivative of Reynolds' force. This drive of ZF shear has been diagnosed in many experiments [23–25] through the Reynolds' stress calculated using floating potential

$$\phi_f = \phi - \Lambda T_e \ , \tag{10}$$

where Λ is the sheath potential coefficient.

The last term in Equation (7) won't be canceled by zonal average, so it is also a possible drive of ZF shear. To study its physical meaning and properties, we decompose $j_\parallel$ using the balance of parallel pressure drop, parallel potential drop and collision,

$$j_\parallel = \frac{e}{\nu_e m_e}\left(\nabla_\parallel p_e - en\nabla_\parallel\phi\right) \ . \tag{11}$$

Large parallel heat conduction leads to $\nabla_\parallel T_e/T_e \ll \nabla_\parallel n/n$, so for Equation (7) we have

$$\begin{aligned}F_\parallel^\dagger &\equiv \frac{\Omega_i}{e}\left\langle\frac{1}{n}\nabla_\parallel j_\parallel\right\rangle \\ &\approx \frac{\Omega_i}{m_e}\left\langle\frac{1}{n}\nabla_\parallel\left[\frac{T_e}{\nu_e}\left(\nabla_\parallel n - en\frac{\nabla_\parallel\phi}{T_e}\right)\right]\right\rangle \ .\end{aligned} \tag{12}$$

Since δn and δT_e are usually in phase, the above approximation would result in a slight loss of total amplitude. In the lowest order of $F_\parallel^\dagger$, the remaining perturbations are $\nabla_\parallel \delta n$, $\nabla_\parallel \delta\phi$ and $\delta(1/n)$. Neglecting $\delta(T_e/\nu_e)$, we define an approximation of $F_\parallel^\dagger$ by

$$F_\parallel \equiv \frac{\Omega_i}{m_e}\left\langle\frac{T_e}{\nu_e}\right\rangle\left\langle\frac{1}{n}\nabla_\parallel\left(\nabla_\parallel n - en\frac{\nabla_\parallel\phi}{T_e}\right)\right\rangle \ . \tag{13}$$

For density and potential perturbations of collisional drift wave (CDW) in linear devices, the amplitude $|\delta\phi/T_e|\,/\,|\delta n/n| \lesssim 1$ and the cross-phase $\xi\left(\tilde{n},\tilde{\phi}\right) < \pi/4$ [26, 27]. Consequently, for weakly adiabatic electrons, one would expect a secondary change of $F_\parallel$ if $\nabla_\parallel\phi$ is neglected

$$F_\parallel \approx G_\parallel \equiv \frac{\Omega_i}{m_e}\left\langle\frac{T_e}{\nu_e}\right\rangle\left\langle\left(\frac{\nabla_\parallel n}{n}\right)^2\right\rangle \ . \tag{14}$$

A typical shear flow growth phase of CSDX is shown in Figure 1, revealing that our approximations in Equations (12) to (14) are basically valid, especially for $r < 3$ cm, where perturbations are much smaller than the corresponding zonal component.

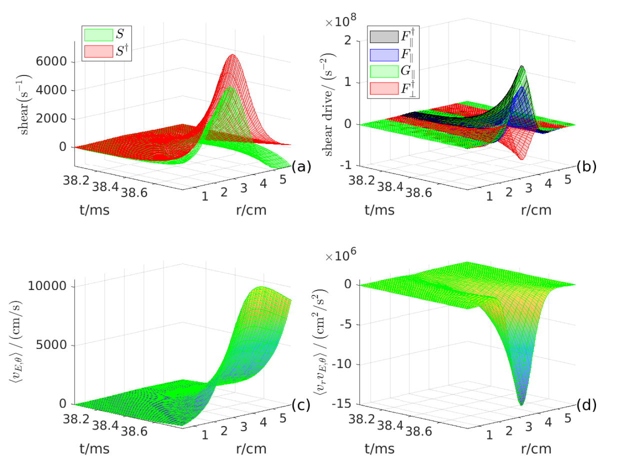

FIG. 1. Simulation result of some zonal-averaged fields in a typical shear flow growth phase. (a) evolution of flow shear, defined in Equation (8). (b) evolution of flow shear drives, defined in Equations (9) and (12) to (14).

As can be seen in Figure 1(a), the flow shear grows globally, with the maximum amplitude near $r \approx 3$ cm, where $\langle n\rangle$ and $\langle T_e\rangle$ has the maximum gradient, and the instability has the maximum intensity. Figure 1(b) shows that, the main drive of zonal flow shear is $F_{\parallel}^{\dagger}$, and $F_{\perp}^{\dagger}$ flattens the flow profile. The resulting growth of $\boldsymbol{E} \times \boldsymbol{B}$ is shown in Figure 1(c), which can be compared to time-delay estimation (TDE) results in [25, 28]. Note that the TDE result would include CDW phase velocity as explained in [?]. Reynolds' stress can be regarded as ZF flux, peaking near the maximum ZF shear location (Figure 1(d)), convecting ZF down its gradient. Equation (14) shows that, the main part of $F_{\parallel}^{\dagger}$, $G_{\parallel}$, is positive definite. At the edge of tokamaks where ν_e is relatively high, the relatively weakly adiabatic electrons would hardly cancel $G_{\parallel}$, so there should always be a finite drive of positive E_r shear.

As a validation of our simulation, we compare our simulation result of Reynolds' stress with experimental observations. For the argon plasma in CSDX, the sheath potential coefficient in Equation (10) is estimated by [29]

$$\Lambda = \frac{1}{2} \ln \left(\frac{m_i}{2\pi m_e} \right) \approx 4.68 \ , \qquad (15)$$

which is significantly larger than deuterium plasmas, making the approximation $\phi \approx \phi_f$ easier to break down. The breaking in our simulation is shown in Figure 2. In spite of a somewhat unknown filter used in experiments, our simulation results of time-averaged synthetic $\langle v_{E,r} v_{E,\theta} \rangle$ and $\langle v_{E,r}^2 \rangle$ agree with experimental observations well [23, 25]. However, when we use plasma potential ϕ, the amplitude of the two profiles reduce significantly, and the Reynolds' stress changes shape.

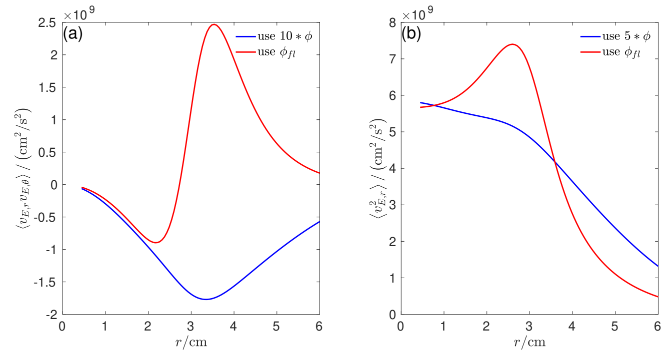

FIG. 2. Simulation result of some zonal and time averaged fields during $t = 9.4 - 50.8$ ms. The blue curves are calculated using multiples of plasma potential, while the red curves are calculated using synthetic floating potential given by Equations (10) and (15). (a) Reynolds' stress and (b) the intensity of radial $\boldsymbol{E} \times \boldsymbol{B}$ velocity perturbations.

[1] X. Li, Z. Guo, and K. Zhao, Plasma Physics and Controlled Fusion **62**, 125018 (2020).

[2] P. H. Diamond, S.-I. Itoh, K. Itoh, and T. S. Hahm, Plasma Physics and Controlled Fusion **47**, R35 (2005).

[3] P. Diamond, C. McDevitt, O. Gürcan, T. Hahm, W. X. Wang, E. Yoon, I. Holod, Z. Lin, V. Naulin, and R. Singh, Nuclear Fusion **49**, 045002 (2009).

[4] P. Diamond, Y. Kosuga, O. Gürcan, C. McDevitt, T. Hahm, N. Fedorczak, J. Rice, W. Wang, S. Ku, J. Kwon, G. Dif-Pradalier, J. Abiteboul, L. Wang, W. Ko, Y. Shi, K. Ida, W. Solomon, H. Jhang, S. Kim, S. Yi, S. Ko, Y. Sarazin, R. Singh, and C. Chang, Nuclear Fusion **53**, 104019 (2013).

[5] S. Chakraborty Thakur, M. Xu, P. Manz, N. Fedorczak, C. Holland, and G. R. Tynan, Physics of Plasmas **20**, 012304 (2013).

[6] M. Xu, G. R. Tynan, C. Holland, Z. Yan, S. H. Muller, and J. H. Yu, Physics of Plasmas **17**, 032311 (2010).

[7] R. J. Hajjar, P. H. Diamond, and G. R. Tynan, Physics of Plasmas **25**, 022301 (2018).

[8] L. Cui, A. Ashourvan, S. C. Thakur, R. Hong, P. H. Diamond, and G. R. Tynan, Physics of Plasmas **23**, 055704 (2016).

[9] M. Xu, G. R. Tynan, C. Holland, Z. Yan, S. H. Muller, and J. H. Yu, Physics of Plasmas **16**, 042312 (2009).

[10] C. Holland, J. H. Yu, A. James, D. Nishijima, M. Shimada, N. Taheri, and G. R. Tynan, Phys. Rev. Lett. **96**, 195002 (2006).

[11] Z. Yan, J. H. Yu, C. Holland, M. Xu, S. H. Müller, and G. R. Tynan, Physics of Plasmas **15**, 092309 (2008).

[12] Z. Yan, M. Xu, P. H. Diamond, C. Holland, S. H. Müller, G. R. Tynan, and J. H. Yu, Phys. Rev. Lett. **104**, 065002 (2010).

[13] P. Vaezi, C. Holland, S. C. Thakur, and G. R. Tynan, Physics of Plasmas **24**, 092310 (2017).

[14] Y. Lang, Z. B. Guo, X. G. Wang, and B. Li, Phys. Rev. E **100**, 033212 (2019).

[15] A. Zeiler, J. F. Drake, and B. Rogers, Physics of Plasmas **4**, 2134 (1997).

[16] P. Ricci, F. D. Halpern, S. Jolliet, J. Loizu, A. Mosetto, A. Fasoli, I. Furno, and C. Theiler, Plasma Physics and Controlled Fusion **54**, 124047 (2012).

[17] M. Held, M. Wiesenberger, R. Kube, and A. Kendl, Nuclear Fusion **58**, 104001 (2018).

[18] J. C. Li and P. H. Diamond, Physics of Plasmas **25**, 062112 (2018).

[19] P. H. Diamond and Y. Kim, Physics of Fluids B: Plasma Physics **3**, 1626 (1991).

[20] S. Chakraborty Thakur, R. Hong, and G. R. Tynan, Review of Scientific Instruments **89**, 10J117 (2018).

[21] A. Hasegawa and M. Wakatani, Phys. Rev. Lett. **50**, 682 (1983).

[22] P. Vaezi, C. Holland, S. C. Thakur, and G. R. Tynan, Physics of Plasmas **24**, 042306 (2017).

[23] Z. Yan, J. H. Yu, C. Holland, M. Xu, S. H. Müller, and G. R. Tynan, Physics of Plasmas **15**, 092309 (2008).

[24] C. Holland, J. H. Yu, A. James, D. Nishijima, M. Shimada, N. Taheri, and G. R. Tynan, Phys. Rev. Lett. **96**, 195002 (2006).

[25] Z. Yan, M. Xu, P. H. Diamond, C. Holland, S. H. Müller, G. R. Tynan, and J. H. Yu, Phys. Rev. Lett. **104**, 065002 (2010).

[26] S. C. Thakur, C. Brandt, L. Cui, J. J. Gosselin, A. D. Light, and G. R. Tynan, Plasma Sources Science and Technology **23**, 044006 (2014).
[27] D. L. Jassby, The Physics of Fluids **15**, 1590 (1972).
[28] Z. Yan, G. R. Tynan, C. Holland, M. Xu, S. H. Müller, and J. H. Yu, Physics of Plasmas **17**, 032302 (2010), https://doi.org/10.1063/1.3322823.
[29] L. Nie, M. Xu, R. Ke, B. Yuan, Y. Wu, J. Cheng, T. Lan, Y. Yu, R. Hong, D. Guo, L. Ting, Y. Dong, Y. Zhang, X. Song, W. Zhong, Z. Wang, A. Sun, J. Xu, W. Chen, L. Yan, X. Zou, and X. D. and, Nuclear Fusion **58**, 036021 (2018).